Structure of ferrofluid nanofilms in homogeneous magnetic fields

Jelena Jordanovic and Sabine H. L. Klapp*
Institut für Theoretische Physik, Fachbereich Physik, Freie Universität Berlin, Arnimallee 14, D-14195 Berlin, Germany
(Received 13 November 2008; published 13 February 2009)

We report molecular dynamics simulations results for model ferrofluid films subject to an external, homogeneous magnetic field directed parallel or perpendicular to the film surfaces. The interactions between the magnetic nanoparticles are modeled via the Stockmayer potential. In a previous study [J. Jordanovic and S. H. L. Klapp, Phys. Rev. Lett. **101**, 038302 (2008)] we have shown that an external field can control the number and internal structure of the layers characterizing the fluid films, in qualitative agreement with experiments. Here we explore the dependence of the layering effects on thermodynamic conditions, and we analyze the results from an energetic (microscopic and macroscopic) perspective. As a special case we investigate a monolayer to bilayer transition induced via a perpendicular field.

DOI: 10.1103/PhysRevE.79.021405 PACS number(s): 82.70.Dd

I. INTRODUCTION

It is now well established that quasi-two-dimensional systems involving dipolar interactions such as thin films of ferrofluids [1,2], magnetic nanoparticles at interfaces [3,4], thin magnetic films [5], but also systems of superparamagnetic [6] or polarizable particles [7] can display a variety of self-organized structures. Examples are the self-assembly into (in-plane) chains [2] and the formation of one- and two-dimensional crystalline structures [7,8] and other patterns in systems with additional external fields [4,5,8–10]. Many of these experimentally observed phenomena can be reproduced by particle-based computer simulations of simple dipolar model fluids. This concerns the chaining [11–15] but also the formation of larger (mesoscale) patterns such as labyrinths and columnar structures [16,17].

Additional phenomena emerge when quasi-two-dimensional systems are somewhat expanded into the third dimension. An immediate effect occurring already for nonpolar particles is the formation of layers of particles. A specific feature for dipolar systems, on the other hand, is that the layer formation can be influenced by magnetic fields directed parallel or perpendicular to the surface. This has been first revealed by neutron reflectometry measurements [18]. In a recent paper [19] we have reported molecular dynamics (MD) simulation results supporting the field effects on dipolar layering. As a model system we used a Stockmayer fluid (involving dipolar and Lennard-Jones interactions) confined between two plane parallel walls. In particular, we have shown that an external perpendicular field can induce new layers in the system, whereas an in-plane field has the opposite effect. Thus, external fields can serve as control parameters for the (surface-initiated) layering.

The purpose of the present paper is to give a more detailed description of our results. In [19] we have concentrated on the role of the surface separation. Here we rather focus on the dependence of the field effects on thermodynamic conditions. To this end we have performed extensive MD simulations of confined Stockmayer fluids at various densities in the liquid phase regime and several values of the external field. Furthermore, we interpret the results in the light of a macroscopic (mean-field) theory and in terms of microscopic energies characterizing the dipolar layers. Moreover, we present results for systems close to two dimensions.

The paper is organized as follows. In Secs. II and III we describe the model system and some technical details of our simulations. A mean-field description of the confined systems is given in Sec. IV. Numerical results are presented in Sec. V, and in Sec. VI we summarize the main findings.

II. MODEL SYSTEM

We consider a Stockmayer (SM) fluid consisting of N spherical particles with embedded, permanent point dipole moments $\boldsymbol{\mu}_i$ $(i=1,\ldots,N)$ located in the center of the spheres. The total interaction between two particles i and j consists of a Lennard-Jones (LJ) and a dipole-dipole (DD) potential. The LJ potential is defined as

$$u_{\mathrm{LJ}}(ij) = 4\epsilon\left[\left(\frac{\sigma}{r_{ij}}\right)^{12} - \left(\frac{\sigma}{r_{ij}}\right)^{6}\right], \tag{2.1}$$

where $r_{ij}=|\mathbf{r}_{ij}|=|\mathbf{r}_i-\mathbf{r}_j|$ is the distance between the particles and σ is their diameter. To save simulation time we truncate and shift the LJ potential at $r_c=2.5\sigma$ [20]. The dipole-dipole interaction is given by

$$u_{\mathrm{DD}}(ij) = \frac{\boldsymbol{\mu}_i\cdot\boldsymbol{\mu}_j}{r_{ij}^3} - 3\frac{(\boldsymbol{\mu}_i\cdot\mathbf{r}_{ij})(\boldsymbol{\mu}_j\cdot\mathbf{r}_{ij})}{r_{ij}^5}. \tag{2.2}$$

Following earlier simulation work on Stockmayer fluids (see, e.g., [21,22]), which are also used as models for systems with electric dipoles, we do not use physical units here.

To model a fluid film we introduce two plane-parallel walls located at $z=\pm L_z/2$, which are infinitely extended in the x-y plane. The fluid-wall potentials affecting particle i are given by an integrated LJ potential [13,23], yielding

*klapp@physik.fu-berlin.de

$$u_{\mathrm{FW}}^{\pm}(i) = \frac{2\pi}{3}\epsilon\left[\frac{2}{15}\left(\frac{\sigma}{\frac{L_z}{2} \pm z_i}\right)^9 - \left(\frac{\sigma}{\frac{L_z}{2} \pm z_i}\right)^3\right], \quad (2.3)$$

where the minus (plus) corresponds to the interaction with the upper (lower) wall. In addition, the particles are subject to an external, homogeneous field $\mathbf{H}$, yielding a potential contribution

$$u_{\mathrm{DF}}(i) = -\boldsymbol{\mu}_i \cdot \mathbf{H}. \quad (2.4)$$

The field direction is chosen to be either perpendicular to the surfaces, i.e., $\mathbf{H}=\mathbf{H}_z=H_z\hat{\mathbf{e}}_z$, or parallel to them, i.e., $\mathbf{H}=\mathbf{H}_\parallel=H_\parallel\hat{\mathbf{e}}_x$ (with $\hat{\mathbf{e}}_\alpha$ being the unity vector in direction α).

III. COMPUTER SIMULATIONS

We perform MD simulations of $N=500$ particles at constant (kinetic) temperature T [20]. The translational and rotational equations of motion are solved via the standard leap-frog algorithm [20], using a time step of $\Delta t^*=0.0025$ with $t^*=\sqrt{\epsilon/m\sigma^2}t$, m being the mass of the particles. The long-range character of the dipole-dipole interaction is handled via a "slab-adapted" version of the three-dimensional Ewald summation [23–25] with conducting boundary conditions parallel to the surfaces and insulating ones in the z direction (the latter are not expected to influence the results qualitatively [26]). The simulations were started from zero-field configurations of confined SM fluids generated as described in a previous study [13]. For small field strengths the systems equilibrate in about 3×10^4 steps, while at higher field strengths even fewer steps are needed since the field suppresses orientational fluctuations. There were no marked differences in the equilibration times between the cases $\mathbf{H}=\mathbf{H}_z$ and $\mathbf{H}=\mathbf{H}_\parallel$.

The simulations were carried out at the reduced temperature $T^*=k_\mathrm{B}T/\epsilon=1.35$ and the reduced dipole moment $\mu^*=\mu/\sqrt{\epsilon\sigma^3}=2.0$. These values correspond to a dipolar coupling parameter of $\lambda=\mu^2/k_\mathrm{B}T\sigma^3=(\mu^*)^2/T^*\approx3.0$. Furthermore, we consider wall separations $L_z^*=L_z/\sigma\leqslant5.0$. The overall reduced density $\rho^*=\rho\sigma^3=N\sigma^3/AL_z$ was set to values between 0.4 and 0.8. The strength of the external field is measured through the parameter $H^*=H\mu/k_\mathrm{B}T$, and we consider field strengths up to $H^*\approx75$. We note that this value is rather high for many real ferrocolloids, which typically consist of nanoparticles with diameters of about 10 nm. The magnetic moment μ is proportional to the particle's volume (see, e.g., [27]). For the typical 10 nm particles one can then infer that the real magnetic field corresponding to $H^*=75$ would be about 3 T, which is indeed very large. On the other hand, the value $H^*\approx75$ can be easily reached for larger particles. Indeed, the particles used in Ref. [2] had a diameter of about 24 nm such that much smaller field strengths of about 0.2 T are required at the same dipole-field coupling strength.

It is also worth to briefly discuss our parameters in the light of what is known theoretically about the phase behavior of confined SM fluids (in zero field). First, the coupling parameter $\lambda\approx3$ is far too small to induce spontaneous magnetization. Such behavior has indeed been found in strongly confined ($L_z^*\approx3$–7), dense systems of dipolar soft spheres, but only at $\lambda\approx7$ [25,28]. Another issue is the condensation transition between vapor and (isotropic) liquid. Indeed, the bulk Stockmayer fluid characterized by $\mu^*=2.0$ has a vapor-liquid critical point at $T_c^*=2.06$ and $\rho_c^*=0.29$ [29]. Vapor-liquid coexistence of confined SM fluids at $\mu^*=2.0$ (and a purely repulsive fluid-wall potential) has been investigated very recently by Richardi *et al.* [16], who employed Gibbs ensemble Monte Carlo simulations. As expected [23], the condensation transition is strongly affected by the spatial confinement. In particular, one observes a narrowing of the coexistence curve on the liquid side [16]. The transition still exists at a wall separation of $L_z^*=6.0$ (smaller values were not considered) and temperatures comparable to the value $T^*=1.35$ chosen here. Taking these results as a reference we expect that our model fluid at $L_z^*=5.0$ (to which most of present results pertain) is in a condensed liquid phase for densities $\rho^*\gtrsim0.5$. Lower densities presumably correspond to states either close to or even within the coexistence line. Note, however, that these densities can still correspond to stable states when the system is subject to a strong perpendicular field, $\mathbf{H}_z$.

Structural quantities

The overall field-induced magnetization is measured by the standard first-rank order parameter

$$P_1 = \frac{1}{N}\sum_{i=1}^{N}|\hat{\boldsymbol{\mu}}_i \cdot \hat{\mathbf{d}}|, \quad (3.1)$$

where $\hat{\boldsymbol{\mu}}_i$ is the unit vector associated with the dipole moment of particle i, and $\hat{\mathbf{d}}$ is the global director of the field-induced (or spontaneous) order. In general, $\hat{\mathbf{d}}$ is defined as the eigenvector corresponding to the largest eigenvalue of the ordering matrix $\mathbf{Q}$ with Cartesian elements $Q_{\alpha\beta}=N^{-1}\Sigma_{i=1}^{N}(3\hat{\mu}_{i,\alpha}\hat{\mu}_{i,\beta}-\delta_{\alpha\beta})/2$ [20]. This definition takes into account the possibility of spontaneous ordering. Indeed, spontaneous magnetization has been observed in dipolar nanofilms characterized by a very large coupling strength [15,25]. In the present work we focus on moderate coupling conditions where the zero-field system is isotropic, and $\hat{\mathbf{d}}$ coincides with the field direction. Perfect alignment along the field corresponds to $P_1=1$.

The surface-induced inhomogeneity of the number density is measured, as usual, by density profiles $\rho(z)=\langle N(z)\rangle/(A\delta z)$ where $N(z)$ is the number of particles in a slice of thickness $\delta z=0.05\sigma$ around z, and A is the box area in the x-y plane. In addition, we consider the local polarization,

$$P_1(z) = \left\langle \frac{\sum_{i=1}^{N(z)} \hat{\boldsymbol{\mu}}_i \cdot \hat{\mathbf{d}}}{N(z)} \right\rangle. \quad (3.2)$$

A typical surface effect revealed by $\rho(z)$ is the formation of layers parallel to the confining walls. The lateral order within these layers is investigated via in-plane ("intra") correlation functions defined as

$$g_{\alpha}^{\mathrm{intra}}(R)=\left\langle \frac{\sum_{i,j(i\neq j)}^{N_{\alpha}}\delta(R-R_{ij})}{N_{\alpha}\rho_{\alpha}2\pi R\Delta R\delta z}\right\rangle, \tag{3.3}$$

where the pairs ij are from the same layer α with N_α particles and a typical thickness δz of about one particle diameter. Also, $R_{ij}=\sqrt{x_{ij}^2+y_{ij}^2}$ is the lateral distance between these particles, and $\Delta R=0.05\sigma$ is a tolerance. The layers are identified from the density profiles [13] by locating the z values of two adjacent minima.

To measure the degree of translational lateral ordering quantitatively we compute the bond-angle order parameters

$$\psi_n=\left\langle \frac{1}{N_\alpha}\sum_{i=1}^{N_\alpha}\frac{1}{N_i^b}\left|\sum_{j=1}^{N_i^b}\exp(in\theta_j)\right|\right\rangle, \tag{3.4}$$

where N_i^b is the number of neighbors of a particle i, and θ_j is the angle of the bond vector $\mathbf{R}_{ij}=(x_{ij},y_{ij})$ between neighboring particles i and j and an arbitrary in-plane axis, e.g., the x axis. Particles i and j are considered as neighbors if their separation R_{ij} is smaller than the distance related to the first minimum of the in-plane pair correlation function $g_\alpha^{\mathrm{intra}}(R)$. We are particularly interested in the order parameters ψ_4 and ψ_6 measuring how close the system is to a perfect square lattice ($\psi_4=1$, $\psi_6=0$) or hexagonal lattice ($\psi_4=0$, $\psi_6=1$). Indeed, hexagonal and squarelike ordering has been observed in two-dimensional (or nearly two-dimensional) systems of paramagnetic particles [6,8].

Finally, the mutual arrangement of particles in neighboring layers α and $\beta\neq\alpha$ is investigated via interlayer correlation functions defined by

$$g_{\alpha\beta}^{\mathrm{inter}}(R)=\left\langle \frac{\sum_{i\in\beta}^{N_\beta}\sum_{j\in\alpha}^{N_\alpha}\delta(R-R_{ij})}{N_\alpha\rho_\alpha 2\pi R\Delta R\delta z_\alpha}\right\rangle. \tag{3.5}$$

IV. MEAN-FIELD THEORY

As a reference for the computer simulations it is instructive to consider the predictions of a simple, mean-field (MF) type of theory. Within this framework the interactions between the particle are taken into account only via an effective field $\mathbf{H}^{\mathrm{MF}}$ acting on each of the otherwise uncorrelated particles. Following earlier work [25], we further assume that the inhomogeneous confined systems can be characterized by a homogeneous singlet density and thus, a homogeneous mean field. The resulting expression for $\mathbf{H}^{\mathrm{MF}}$ consists of (i) a bulklike ("Lorentz") field $(4\pi/3V)\mathbf{M}$ (with $\mathbf{M}=\langle\Sigma_{i=1}^N\boldsymbol{\mu}_i\rangle$ being the total magnetization), (ii) surface corrections to the Lorentz field, and (iii) a "demagnetizing field" $\mathbf{H}^{\mathrm{DM}}$ which depends on the direction of the external field, $\mathbf{H}$. In particular, if $\mathbf{H}=\mathbf{H}_z$, the field-induced magnetization gives rise to surface "charges" which generate, in turn, a demagnetizing field of strength $\mathbf{H}^{\mathrm{DM}}=-(4\pi/V)M_z\hat{\mathbf{e}}_z$ (where M_z is the z component of the magnetization). We note that, for the geometry and field direction considered, the demagnetizing field exists irrespective of the boundary conditions in the z direction [26]. On the other hand, $\mathbf{H}^{\mathrm{DM}}=\mathbf{0}$ in the case of a parallel external field, because no surface charges are induced. Taken altogether, the mean-field contributions are [25]

$$\mathbf{H}_z^{\mathrm{MF}}=-\rho\mu\left(\frac{8\pi}{3}-\pi\frac{\sigma}{L_z}\right)P_1\hat{\mathbf{e}}_z,$$

$$\mathbf{H}_{\parallel}^{\mathrm{MF}}=\rho\mu\left(\frac{4\pi}{3}-\frac{\pi}{2}\frac{\sigma}{L_z}\right)P_1\hat{\mathbf{e}}_x. \tag{4.1}$$

In Eq. (4.1) we have used the ansatz $\mathbf{M}=N\mu P_1\hat{\mathbf{d}}$. The appearance of the terms $\propto\sigma/L_z$ reflect the reduction of the mean fields due to the presence of surfaces. Indeed, for a bulk system without any boundaries the mean field reduces to the Lorentz field, that is, $|\mathbf{H}^{\mathrm{MF}}|=\rho\mu(4\pi/3)P_1$. In all cases, the total field acting on a particle is $\mathbf{H}_{z(\|)}^{\mathrm{tot}}=\mathbf{H}_{z(\|)}^{\mathrm{MF}}+\mathbf{H}_{z(\|)}$.

Given the above mean-field expressions we can calculate the magnetization order parameter P_1 as a function of the field strength (and the thermodynamic parameters). Recalling that the mean-field system is uncorrelated, the probability for a dipole to orient along a given direction $\boldsymbol{\mu}$ is determined by the Boltzmann factor $\propto\exp[-\beta U(\boldsymbol{\mu})]$ with $U(\boldsymbol{\mu})=-\boldsymbol{\mu}\cdot\mathbf{H}^{\mathrm{tot}}$. Thus, we arrive at the MF equation

$$P_1=\frac{\int d\omega\hat{\boldsymbol{\mu}}(\omega)\cdot\hat{\mathbf{d}}\exp[\beta\boldsymbol{\mu}(\omega)\cdot\mathbf{H}^{\mathrm{tot}}]}{\int d\omega\exp[\beta\boldsymbol{\mu}(\omega)\cdot\mathbf{H}^{\mathrm{tot}}]}, \tag{4.2}$$

where $\int d\omega=\int_0^{2\pi}d\varphi\int_0^{\pi}d\theta\sin\theta$. For the perpendicular field ($\hat{\mathbf{d}}=\hat{\mathbf{e}}_z$) one has $\hat{\boldsymbol{\mu}}(\omega)\cdot\hat{\mathbf{e}}_z=\cos\theta$ and $\boldsymbol{\mu}(\omega)\cdot\mathbf{H}^{\mathrm{tot}}=\mu H^{\mathrm{tot}}\cos\theta$, such that the integrand does not depend on φ. The integral then leads to the standard Langevin function

$$P_1|_{\mathbf{H}_z}=\mathcal{L}[f(H_z,P_1)], \tag{4.3}$$

where $\mathcal{L}(y)=\coth(y)-1/y$ and $f(H_z,P_1)=\beta\mu H_z-\beta\rho\mu^2P_1(8\pi/3-\pi\sigma/L_z)$.

For the case of a parallel field we use Eq. (4.2) with $\hat{\mathbf{d}}=\hat{\mathbf{e}}_x$. Using $\hat{\boldsymbol{\mu}}(\omega)\cdot\hat{\mathbf{e}}_x=\sin\theta\cos\varphi$, the MF expression for order parameter becomes

$$P_1|_{\mathbf{H}_{\parallel}}=\frac{\int_0^{2\pi}d\varphi\int_0^{\pi}d\theta\sin^2\theta\cos\varphi\exp[\sin\theta\cos\varphi g(H_{\parallel},P_1)]}{\int_0^{2\pi}d\varphi\int_0^{\pi}d\theta\sin\theta\exp[\sin\theta\cos\varphi g(H_{\parallel},P_1)]}, \tag{4.4}$$

where $g(H_{\parallel},P_1)=\beta\mu H_{\parallel}+\beta\rho\mu^2P_1(4\pi/3-\frac{1}{2}\pi\sigma/L_z)$. Performing first the integration over φ we obtain

$$P_1|_{\mathbf{H}_\parallel} = \frac{\int_0^\pi d\theta \sin^2\theta \mathcal{I}_1[\sin\theta g(H_\parallel, P_1)]}{\int_0^\pi d\theta \sin\theta \mathcal{I}_0[\sin\theta g(H_\parallel, P_1)]}, \quad (4.5)$$

where $\mathcal{I}_n(x)$ is the modified Bessel function of order n.

A further simplification of the case of a parallel field occurs when we assume that the particles orient along in-plane directions already without the external field. This assumption is indeed not unreasonable in strongly coupled systems where the preference of in-plane orientations is well established [25]. Neglecting any perpendicular orientations, that is, assuming $\sin\theta = 1$, Eq. (4.5) transforms into

$$P_1|_{\mathbf{H}_\parallel, \theta=\pi/2} = \frac{\mathcal{I}_1[g(H_\parallel, P_1)]}{\mathcal{I}_0[g(H_\parallel, P_1)]}. \quad (4.6)$$

For completeness we also give the corresponding bulk relation, where

$$P_1|_{\text{bulk}} = \mathcal{L}[e(H, P_1)], \quad (4.7)$$

with $e(H, P_1) = \beta\mu H + \beta\rho\mu^2 P_1 4\pi/3$.

The MF equations (4.3) and (4.5)–(4.7) form self-consistency relations for the order parameter P_1, which can be easily solved numerically. Representative results are given in Sec. V A.

V. RESULTS

A. Global order induced by external fields

We start by analyzing the overall field-induced magnetization measured by the order parameter P_1 in the confined SM fluid films. As an example we choose the wall separation $L_z^* = 5.0$. Simulation data for P_1 as function of a parallel or perpendicular magnetic field are plotted in Fig. 1, where we have included corresponding bulk data as a reference. For all systems, the small nonzero values of P_1 directly at $H = 0$ are expected due to the finite size of our simulation system.

Considering first the confined SM fluid in a parallel external field, we see from the simulation data in Fig. 1 that already small values of $H_\parallel^*$ induce a very large magnetization. In other words, the zero-field susceptibility with respect to a parallel field (which could be calculated from the fluctuations of the total dipole moment in parallel directions [30]) is large. In the present study we did not explicitly calculate the susceptibility due to the large simulation times required to obtain convergent results [30].

Interestingly, in the range $H_\parallel^* \lesssim 5$ the confined system responds even more pronouncedly than its bulk counterpart. This is because the dipolar particles in the film prefer in-plane directions already in zero field [13], thereby enhancing the possibility of energetically favorable head-to-tail arrangements. Moreover, there is no macroscopic demagnetizing field (see Sec. IV). These trends are, at least to some extent, reflected by the results of the MF theory included in Fig. 1. Considering a fixed, small field strength (such as $H_\parallel^* = 2$) and focussing on parallel fields, we see that Eq. (4.5) predicts a slightly smaller order parameter than the corresponding bulk relation [see Eq. (4.7)]. This decrease occurs because the mean field in the pore is slightly reduced (due to the excluded volume at the surfaces), while the orientational fluctuations are treated on the same footing for the two systems (bulk and pore). Different behavior is predicted by Eq. (4.6), which takes into account the surface-induced restriction of dipole fluctuations. It follows that the confined (MF) system responds more strongly to $\mathbf{H}_\parallel$ than the bulk, in qualitative agreement with the simulation results. Quantitatively, however, all the MF equations yield poor results. In particular, the MF theory predicts spontaneous magnetization as seen from the nonzero values of P_1 in the limit $H_\parallel^* \to 0$. This indicates that the MF approach strongly overestimates the tendency of the dipolar interactions to form ferromagnetic phases, as expected from previous studies (see, e.g., Ref. [25]).

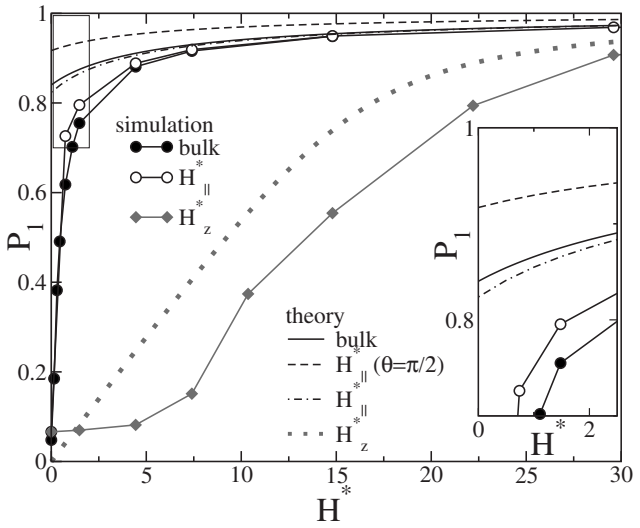

FIG. 1. Global order parameter as a function of the external field at $\rho^* = 0.6$. Simulation and MF results for the confined ($L_z^* = 5.0$) and bulk system are denoted by symbols and lines, respectively. The inset shows the behavior of P_1 for small fields on an expanded scale.

Coming back to the simulation results for $\mathbf{H}_\parallel$, the pronounced response to small fields is also indicated by the behavior of the mean dipolar energy. The latter is plotted in Fig. 2 (without the contribution from the external field). Upon switching on the parallel field, the energy quickly decreases, very similar to what is found in the corresponding bulk system. The decrease indicates that the particles can arrange better and better in energetically "comfortable" configurations. This aspect will be discussed in more detail in Sec. V C.

Considering now the simulation data for a perpendicular field we observe from Fig. 1 entirely different behavior. Increasing H_z^* from zero the magnetization is essentially negligible up to $H^* \approx 7$ (in other words, the zero-field susceptibility is very low for perpendicular fields [30]). Only for larger fields the order parameter achieves significant values, and saturation only occurs for $H_z^* \gtrsim 30$. The behavior of the function $P_1(H_z^*)$ thus reflects that there is a strong "competition"

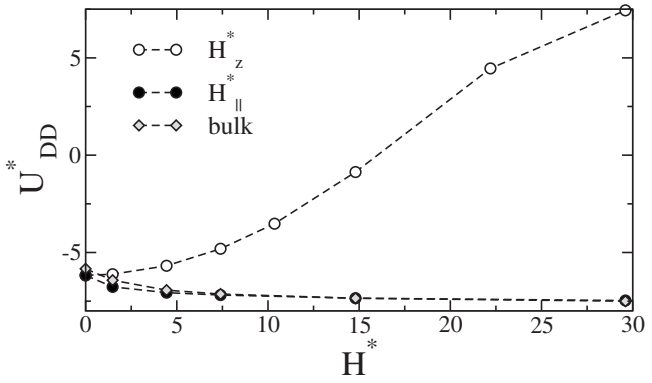

FIG. 2. Simulation data for the total dipolar energy U_{DD}/N at $\rho^*=0.6$, $L_z^*=5.0$, and two directions of the external field. Included are results for the bulk system.

between the external field, which tends to align the particles normal to the surfaces, and the surface-induced preference of in-plane orientations. Our MF approach [see Eq. (4.3)] is unable to reproduce this latter effect, it only takes into account the macroscopic demagnetizing field (see Sec. IV). Still, we observe from Fig. 1 that the MF order parameter for a finite H_z^* is much smaller than its bulk counterpart, in qualitative agreement with the MD data.

The behavior of the corresponding mean dipolar energy (see Fig. 2) furthermore shows how the external field renders the system more and more repulsive as a whole. Interestingly, U_{DD} changes sign just in the range of field strengths where P_1 increases markedly. In Figs. 1 and 2 the results are presented only for one thermodynamic state. It seems plausible that the "threshold" range where an external perpendicular field can overcome the barrier depends on the density and dipole coupling. This issue will be discussed in Sec. V B.

B. Structural changes induced by a perpendicular field

1. Layering

We now discuss microscopic properties of the confined films, focussing first on layering effects. In an earlier study [19] we have demonstrated that the corresponding oscillations of the density profiles $\rho^*(z)$ and, in particular, the resulting number of layers can be enhanced by an external field $\mathbf{H}_z$. The main focus of Ref. [19] has been the dependence of the field-induced layer formation on the surface separation. Here we rather explore the role of the (average) density ρ^* and the dipolar coupling parameter, λ.

An interesting question is which field strengths H_z^* are required to form an additional layer. Not surprisingly, the layer generation is closely related to the degree of field-induced magnetization which, in turn, depends on the density (and coupling strength). Results for the global order parameter P_1 as a function of H_z^* are plotted in Fig. 3(a). All curves display a thresholdlike behavior in the sense that P_1 starts to increase from zero only when H_z^* has significant nonzero values. Moreover, at given finite field, the magnetization at a given value of H_z^* is the larger, the smaller ρ^* is. This behavior is consistent with the macroscopic theory (see Sec. IV) predicting that the demagnetizing field and, thus, the mean field $\mathbf{H}^{MF}$ acting against the external field are proportional to the density [see Eqs. (4.1)]. Therefore, the total field at given H_z^* decreases with ρ^*. Furthermore, lower density implies that the surface-induced in-plane ordering (not captured by the MF approach) is less pronounced.

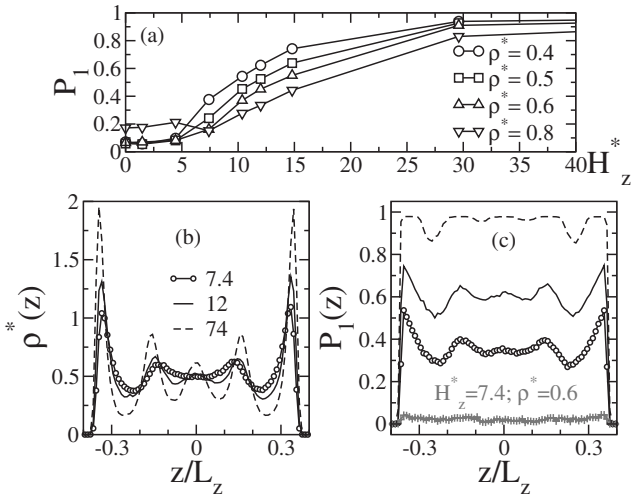

FIG. 3. (a) Global order parameter as function of the field strength at different densities ($L_z^*=5.0$). Parts (b) and (c) show the density and magnetization profiles at $\rho^*=0.4$. For comparison, (c) includes data at $H_z^*=7.4$ and $\rho^*=0.6$ (see bottom).

Analyzing now the curves $P_1(H_z^*)$ in terms of layer formation we find that the new layer typically appears when $P_1 \approx 0.4-0.5$. This corresponds to field strengths of $H_z^* \approx 8$ (at $\rho^*=0.4$) up to $H_z^* \approx 12$ (at $\rho^*=0.6$). Typical results for density profiles at the average density $\rho^*=0.4$ are shown in Fig. 3(b). In the small external field $H_z^* \approx 7$ we observe (as at $H^*=0$) four maxima in $\rho^*(z)$ indicating four layers in the system. The number of four is expected at the present wall separation $L_z^*=5$ and the fact that the fluid-wall interaction defined in Eq. (2.3) disfavors the particles to access the surfaces closer than $\approx\sigma/2$. Different behavior is found already at $H_z^*=12$ where the density profile now reveals a fifth layer in the system. At the same time, the separation between the layers is reduced compared to the low-field case. The layer formation becomes even more pronounced at $H_z^*=74$, as reflected by the strong increase of peak heights. A similar layer creation (at $L_z^*=5.0$) occurs at the average density $\rho^*=0.6$ [19].

In Fig. 3(c) we plot additionally the order parameter $P_1(z)$ [see Eq. (3.2)] for several field strengths at $\rho^*=0.4$. Interestingly, there is some local parallel order even at small fields (e.g., $H_z^*=7.4$) where the global order parameter P_1 is very small. We also see that a denser system ($\rho^*=0.6$) displays essentially no local order at this field, illustrating the density effect mentioned already before. Upon increasing H_z^*, $P_1(z)$ develops oscillations mimicking essentially those in $\rho^*(z)$. We note that, by definition, $P_1(z)$ does not depend on the local number of particles. Therefore, the large peak heights of $P_1(z)$ appearing in the contact zones signal that the field-

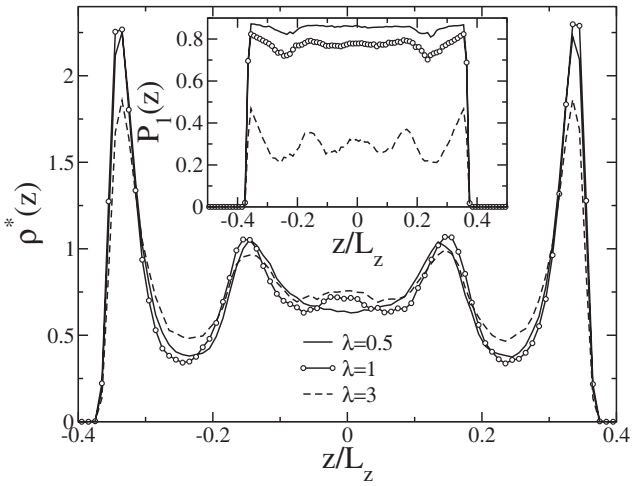

FIG. 4. Density profiles at $\rho^*=0.6$, $H_z^*=10$, and different dipolar coupling parameters λ. The inset shows corresponding magnetization profiles.

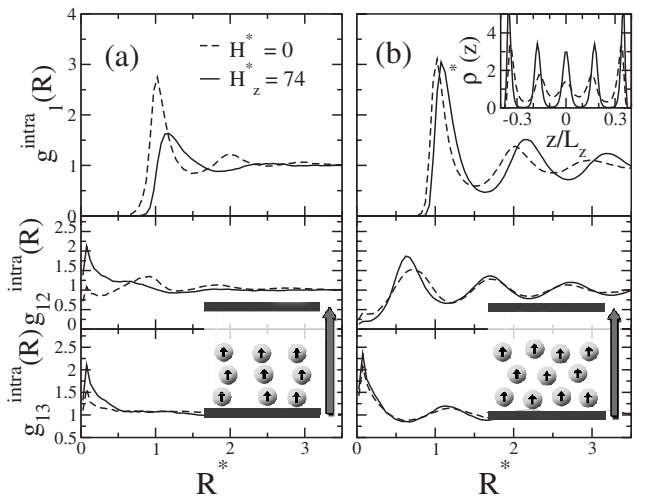

FIG. 5. Interlayer- and intralayer correlation functions at (a) $\rho^*=0.4$ and (b) $\rho^*=0.8$ in zero field and in a perpendicular field. Top, in-plane (contact layer 1); middle, interlayer 1 vs 2; bottom, interlayer 1 vs 3. Included are sketches of the particle arrangements as suggested by the correlations. The inset in the top part of (b) additionally shows the density profile for $\rho^*=0.8$ at zero and perpendicular field.

induced alignment is most pronounced close to the walls, rather than in the middle of the slit. Finally, at the largest field considered ($H_z^*=74$) the system is nearly fully aligned throughout the slit.

So far we have considered systems with a dipolar coupling parameter of $\lambda \approx 3$. We close this paragraph with a brief discussion of layer formation at smaller coupling strengths (higher values of λ are not considered due to the possible appearance of spontaneous polarization [28]). We specialize to the case $\rho^*=0.6$ and $H_z^*=10$. Density profiles for various values of λ are plotted in Fig. 4, where we have included corresponding magnetization profiles. At $\lambda \approx 3$ we observe just the onset of a new layer forming in addition to the four layers present at $H=0$, and the (local) polarization is still rather small. This is different at $\lambda=1$ where the fifth layer is clearly visible and the particles are strongly aligned in spite of the rather small field strength considered. Thus, decreasing λ has a similar effect as decreasing the average density, for the same reasons as discussed before: Decrease of the demagnetization field and the surface-induced preference of in-plane orientations. We found, however, that there is lower limit of λ below which field-induced layer formation becomes impossible. An example is the system at $\lambda=0.5$ for which the density profile reveals only four layers. At the same time, the magnetization in this system is very high. Indeed, the limit $\lambda \to 0$ at fixed H corresponds to a system in which each particle still interacts with the external field, but the interaction between the particles is rather LJ-like. Therefore, the repulsion between the aligned dipoles in a layer vanishes, and the external field does not trigger formation of a new layer. The role of repulsion will be discussed in more detailed below.

2. Lateral ordering

To illustrate the lateral ordering of the confined particles in strong perpendicular fields we present in Fig. 5 results for the intralayer and interlayer correlation functions defined in Eqs. (3.3) and (3.5). At the lower density $\rho^*=0.4$ [see Fig. 5(a)] the most prominent field-induced effect on $g_1^{\text{intra}}(R)$ is a shift of the first peak from $R^* \approx 1$ (zero field) to $R^* \approx 1.2$, indicating a significant increase of the nearest-neighbor distance within the layer. This is reasonable since the field-induced alignment of the dipole moments in side-by-side configurations induces repulsive interactions and is thus energetically unfavorable. At the same time, the maximum of the correlation function $g_{12}^{\text{inter}}(R)$ moves from $R^* \approx 0.9$ ($H=0$) to $R^* \approx 0.1$ ($H_z^*=74$). Thus, looking from a particle in layer 1 (contact layer), its nearest neighbor in the adjacent layer 2 is "pulled" beneath. Similar behavior is reflected by the correlation function between layers 1 and 3 [see bottom of Fig. 5(a)]. We conclude that, at the moderate density considered ($\rho^*=0.4$), the external field yields head-to-tail-like configurations in vertical directions as illustrated by the sketch in the bottom of Fig. 5(a). Indeed, the observation of vertical chains is what one may have expected just from the properties of the dipolar interaction. Nonetheless, a different vertical structure is found in denser systems, as we have shown already in [19] for the case $\rho^*=0.6$. Here we focus on the even larger density $\rho^*=0.8$, where the external field is actually unable to generate a new layer at the chosen wall separation $L_z^*=5.0$ [see the density profiles plotted in the inset of Fig. 5(b)]. Results for the lateral correlations are plotted in the main part of Fig. 5(b). We observe again a shift of the first peak of the intralayer correlation function (top) which is, not surprisingly, much less pronounced than at lower densities. More interestingly, the interlayer correlation functions now reveal formation of a "zig-zag" pattern in vertical directions. Thus, particles in layer 2 are laterally displaced against those in layer 1, whereas those in layer 3 sit on top of those in layer 1 [see sketch in the bottom of Fig. 5(b)]. Very similar behavior has been found at $\rho^*=0.6$ [19]. The appearance of "zig-zag" rather than a chain patterns at

TABLE I. Intralayer and interlayer dipolar energies per particle in zero field and a strong perpendicular field at three densities.

ρ^*	H_z^*	$\tilde{U}_{DD}^1$	$\tilde{U}_{DD}^2$	$\tilde{U}_{DD}^3$	$\tilde{U}_{DD}^{12}$	$\tilde{U}_{DD}^{23}$	$\tilde{U}_{DD}^{13}$
0.4	0	−3.29	−2.71	−2.69	−0.73	−0.81	−0.07
0.4	74	5.49	4.88	4.80	0.06	−0.07	−0.01
0.6	0	−4.04	−3.24	−3.22	−0.77	−0.83	−0.08
0.6	74	8.60	8.02	7.71	0.26	0.34	−0.01
0.8	0	−4.88	−3.14	−2.47	−0.69	−0.82	−0.12
0.8	74	12.29	12.08	11.98	0.30	0.33	−0.0003

TABLE II. Bond-order parameters characterizing the contact layers in zero field and a strong perpendicular field at $\rho^*=0.6$ and $\rho^*=0.8$ (wall separation $L_z^*=5.0$). Included are the average numbers of neighbors.

ρ^*	H_z^*	Ψ_4	Ψ_6	N_b
0.6	0	0.36	0.53	4.37
0.6	74	0.28	0.46	5.33
0.8	0	0.28	0.54	5.09
0.8	74	0.21	0.55	5.7

higher densities can be understood from the fact that the layer spacing is smaller than a particle diameter (e.g., $\Delta z \approx 0.9\sigma$ at $\rho^*=0.8$). Taken altogether, the resulting local structure resembles somewhat the body-centered tetragonal structure found in electrorheological fluids [31] and also in spontaneously ordered dipolar fluids at high densities [32]. We note, however, that the positional effects indicated by the correlation functions in Fig. 5(b) are clearly restricted to a short-range scale.

We next consider the mean dipolar energies within and in between the layers [see Eqs. (A1) and (A3), respectively]. Results are given in Table I. For all three densities considered the intralayer and interlayer energies in zero field are negative, consistent with the negative value of the overall dipolar energy in the liquid phase (see Fig. 2 for data at $\rho^*=0.6$). From Table I we observe, in particular, that the energy is lowest in the contact layer (labeled 1). This is because close to the surfaces the local arrangements of the dipoles into in-plane clusters is most pronounced [13]. In a perpendicular external field, all the intralayer energies become positive due to field-induced alignment of the particles (note that the systems are essentially fully magnetized at the high field strength considered, see Fig. 3). It is interesting, however, that the repulsion within the inner layers (2 and 3) is markedly lower than at the boundaries, and this holds for all densities considered. The smaller repulsion can be understood from the fact that the inner layers are somewhat thicker than the contact layer (e.g., at $\rho^*=0.8$, we have $\Delta z \approx 0.95\sigma$ in the first inner layer as compared to $\Delta z \approx 0.55\sigma$ at contact [see inset of Fig. 5(b)]). In other words, particles in the contact layer are more strongly "localized" at a given value of z, whereas the distribution in the inner layers is somewhat smeared. The latter feature yields a softening of the repulsion.

Finally, it is an interesting question whether the field $\mathbf{H}_z$ can induce crystalline order within the layers. Indeed, experiments involving two-dimensional systems of superparamagnetic colloids [6] have shown that an external field normal to the surface generates hexagonal ordering. Motivated by these findings we have calculated bond-order parameters as defined in Eq. (3.4), focussing on the systems with average densities $\rho^*=0.6$ and $\rho^*=0.8$. It turns out, however, that even for these rather dense systems the degree of translational order is small. This is seen from Table II, where we summarize results obtained for the contact layers. Both at $\rho^*=0.6$ and $\rho^*=0.8$ the local surrounding of a particle in zero field resembles that in a hexagonal lattice, as reflected by the somewhat higher values of Ψ_6 as compared to Ψ_4. Switching on a strong perpendicular field does not alter the order parameters significantly. Thus we conclude that there is no field-induced crystallization at the conditions considered.

3. Field-induced monolayer to bilayer transition

Recent experiments [8] of thin films of paramagnetic particles in perpendicular fields have shown that such systems can form interesting patterns such as labyrinths as well as cubic and hexagonal structures. These patterns occur when the film thickness (determined by the separation of two parallel, confining glass plates) is of the order of 1.5 particle diameter. Due to the slightly enhanced space (as compared to a true monolayer) the resulting dipolar interactions are still repulsive, but strongly softened as compared to the r^{-3} repulsion of two aligned dipolar which stand precisely side by side. The resulting "core softening" is indeed believed to be one of the main features yielding pattern formation [33].

Inspired by the above-mentioned experiments [8] we have performed some calculations of our model system (which involves permanent dipoles) at $L_z^*=2.0$ and $\rho^*=0.4$. Corresponding density profiles are shown in Fig. 6(a). In zero field, the density profile reflects the presence of a single layer. Its soft shape indicates some freedom of the particles to move in vertical direction; the resulting situation thus

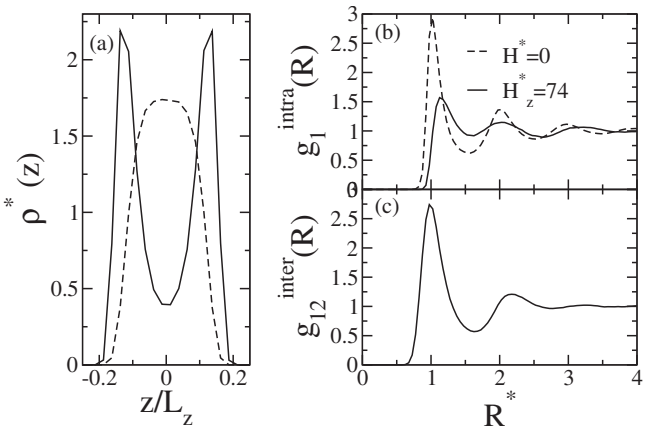

FIG. 6. Density profiles (a) and correlation functions (b) and (c) at $L_z^*=2.0$ in zero field (monolayer) and in a perpendicular field (bilayer). The overall density is $\rho^*=0.4$.

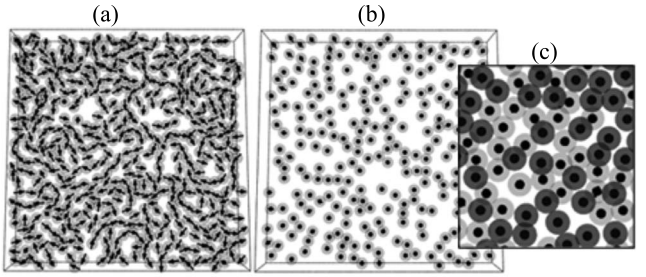

FIG. 7. "Snapshots" of a system at $L_z^*=2.0$ ($\rho^*=0.4$) in zero field (a) and at $H_z^*=74$ (b) and (c).

becomes comparable to that in the experiments [8]. The corresponding MD snapshot in Fig. 7(a) reveals that the particles organize into (short) chainlike structures, as expected in systems of permanent dipoles close to two dimensions (see, e.g., [2,14]). In a strong perpendicular field the structure becomes entirely different. First, the system now consists of two layers [see the density profile in Fig. 6(a)], indicating that the field has induced a transition from a monolayer to a bilayer. The second main effect of the field is the formation of an inhomogeneous lateral structure. Indeed, inspecting the snapshots in Figs. 7(b) and 7(c) we see within each layer a chainlike structure characterized by locally aligned, short strings. Notice that the two layers of the present system are so close to each other (layer spacing $\approx 0.55\sigma$) that the particles cannot arrange on top of each other (forming dipolar pairs in field direction) but are rather displaced. This is also reflected by the positions of the first peaks of the intralayer and interlayer correlation functions plotted in Figs. 6(b) and 6(c).

Similar chainlike structures have been found in the aforementioned experiments [8] on superparamagnetic particles. Indeed, the area packing fraction in our simulations $\eta^{\text{layer}} = (\pi/4)N^{\text{layer}}\sigma^2/A \approx 0.32$ is comparable to the corresponding packing fraction in the experiment. Moreover, inhomogeneous patterns and labyrinths have also been observed in experiments of ferromagnetic nanoparticles evaporated at a surface [3,4]. These effects have recently been simulated by MC simulations [16] of a SM model system very similar to ours. However, the densities considered in [16] were within a gas-liquid coexistence region, contrary to the liquidlike densities considered here. Moreover, the wall separations chosen in [16] were significantly larger (typically $L_z^*=10$). We suspect that these are the main reasons that we do not see labyrinth (and other mesoscale) structures in our system.

C. Impact of a parallel field

As demonstrated in our earlier study [19], external fields can also be used to destroy layers or, at least, to strongly soften the density profile. This is achieved by choosing the field direction within the plane of the film surfaces. Here we discuss in more detail the microscopic effects induced by a parallel field.

As a typical example we consider in Fig. 8 results for the density profile and the local magnetization at $\rho^*=0.8$ and $L_z^*=5.0$. The zero-field system has five layers [see Fig. 8(a)].

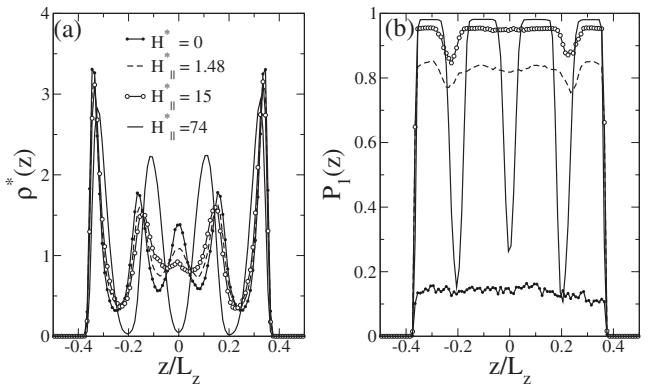

FIG. 8. (a) Density profile and (b) local magnetization at $\rho^*=0.8$, $L_z^*=5.0$, and various strength of the parallel field.

Switching on the parallel field one observes that the middle peak first decreases ($H_\parallel^*=1.48$) and then vanishes at $H_\parallel^*=15$. The result is a plateaulike region between the remaining inner peaks. Increasing $H_\parallel^*$ even further the plateau disappears, while at the same time, the four remaining peaks become more and more pronounced. Finally, at $H_\parallel^*=74$ we observe four well-defined layers which seem completely separated from each other [in the sense that $\rho(z)\approx 0$ between the peaks]. In other words, at very large parallel fields the system becomes solidlike in out-of-plane direction. The development of a solidlike structure is also reflected by the local magnetization plotted in Fig. 8(b).

We now examine the lateral correlation functions, results for which are plotted in Fig. 9. As seen from $g_1^{\text{intra}}(R)$, the parallel field strongly enhances the height of the peaks and renders the general shape somewhat irregular as compared to the situation at $H=0$. In particular, the broadening and increase of the second peak may be interpreted as the beginning of a split-off, a typical phenomenon close to in-plane solidification. The strong degree of local translational order is also visible from the bond-order parameters summarized

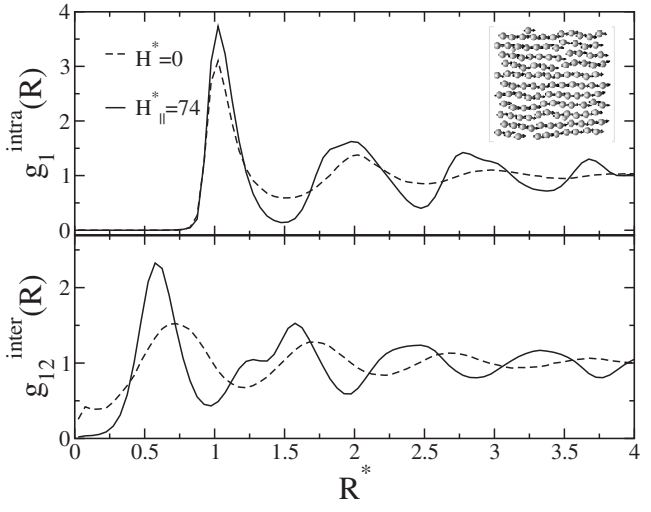

FIG. 9. (a) Intralayer correlation function in contact layer 1 and (b) interlayer correlations between layers 1 and 2 in zero field and in a strong parallel field ($\rho^*=0.8$, $L_z^*=5.0$).

TABLE III. Bond-order parameters characterizing the contact layers in zero field and in a strong parallel field at $\rho^*=0.8$ ($L_z^*=5.0$). Included are the average numbers of neighbors.

ρ^*	H_z^*	Ψ_4	Ψ_6	N_b
0.8	0	0.28	0.53	5.1
0.8	74	0.16	0.77	5.9

TABLE IV. Intralayer and interlayer dipolar energies in zero field and in a strong parallel field at $\rho^*=0.8$ ($L_z^*=5.0$).

ρ^*	$H_\parallel^*$	$\tilde{U}_{\mathrm{DD}}^1$	$\tilde{U}_{\mathrm{DD}}^2$	$\tilde{U}_{\mathrm{DD}}^3$	$\tilde{U}_{\mathrm{DD}}^{12}$	$\tilde{U}_{\mathrm{DD}}^{23}$	$\tilde{U}_{\mathrm{DD}}^{13}$
0.8	0	−4.88	−3.14	−2.47	−0.69	−0.82	−0.12
0.8	74	−8.74	−8.91	−8.96	−0.13	−0.15	−0.002

in Table III. We find that the field generates, in particular, a significant increase of the order parameter Ψ_6 measuring the degree of hexagonal in-plane order. This finding is consistent with the visual impression from the MD snapshot included in Fig. 9(a). One clearly recognizes the formation of long, essentially straight chains in field direction, which are shifted relatively to one other. Due to the shift, the energy between neighboring aligned chains becomes attractive [31]. In fact, the shifted chains are a typical arrangement found in aligned two-dimensional (2D) dipolar systems [2]. In addition, there are also pronounced translational correlations between the layers. Indeed, as seen from the function $g_{12}^{\mathrm{inter}}(R)$ plotted in Fig. 9(b), the parallel field yields a shift of the first peak towards smaller separations, supplemented by a splitting of the second peak. Thus, the chains in the adjacent layers are again shifted relative to one another.

We note that the mutual arrangement of chains in adjacent layers has become possible only because the layer separation in the strong parallel field has enlarged ($\Delta z \approx 1.05\sigma$) relative to that in zero field ($\Delta z \approx 0.9\sigma$). This increase is, of course, a direct consequence of the destruction of a layer already observed from the density profile [see Fig. 8(a)]. In other words, the "microscopic" reason for the observed layer destruction is the formation of a chained, solidlike structure both in the plane of the surfaces and perpendicular to them.

Finally, the fact that the observed chain structure is indeed energetically favorable is also reflected by the intralayer and interlayer dipolar energies, which are given in Table IV. One recognizes, on the one hand, an overall decrease of the energy (as compared to the case $H=0$), in qualitative agreement with the data plotted in Fig. 2 for $\rho^*=0.6$. The energy loss is particularly pronounced within the layers due to the formation of the energetically favorable chain structure. Furthermore, the interaction between the layers is also negative, indicating that the mutual arrangement of the layers indeed optimizes the systems. The smaller values (as compared to those at $H=0$) just follow from the fact that the layer spacing has increased by application of the parallel field.

VI. CONCLUSIONS

In this paper we have analyzed the influence of homogeneous magnetic fields on the internal (lateral) structure of dipolar nanofilms. We have shown that the field-induced effects on the layering already reported in [19] are not specific for a particular thermodynamic state. Rather they are typical for a broad range of densities in the liquid phase. Nevertheless, there are some remarkable, density-dependent effects. First, in perpendicular fields, the density determines the "threshold" field strength above which the field can create a new layer. The underlying relation between density and magnetization is qualitatively reproduced by the predictions of a simple mean-field theory. Second, regarding the internal structure (in strong perpendicular fields), the particles arrange into head-to-tail-like vertical structures at moderate densities, but into "zig-zag" patterns at higher densities. It is remarkable, though, that even at the highest density considered the translational structure in lateral directions (and strong perpendicular fields) is fluidlike, contrary to what is seen in two-dimensional systems of paramagnetic particles [6]. Third, by applying a parallel field at large densities one can induce, at least on a local scale, a crystallization of the system. In particular, we observed the formation of chained, hexagonal structures characterized by large bond-order parameters Ψ_6.

A further aspect explored in this work concerns the structure found in very thin films close to two dimensions, which are subject to a strong perpendicular field. Here we observed highly inhomogeneous lateral patterns resembling the "chain state" reported in a recent experimental study of core-softened colloids [8].

Starting from the present study, an immediate question concerns the role of the (isotropic) attractive interactions in our Stockmayer model for the field-induced layer formation and destruction. Moreover, given the complexity of the structural effects induced by homogeneous magnetic fields, it will be interesting to consider inhomogeneities and also dynamical properties such as diffusion in external fields. Work along these directions is under way.

ACKNOWLEDGMENT

Financial support from the German Science Foundation via the SFB448 "Mesoscopically structured composites" (project B6) is gratefully acknowledged.

APPENDIX: DIPOLAR ENERGIES IN AND IN BETWEEN THE LAYERS

In order to define expressions for the average dipolar energies within a layer (U_{DD}^{α}) and in between two layers ($U_{\mathrm{DD}}^{\alpha\beta}$, with $\alpha \neq \beta$) we start from the full dipolar energy as described via the slab-adapted three-dimenionsional Ewald sum (see, e.g., [25]). Separating the total Ewald sum into subsets, we obtain for the intralayer energy per particle

$$\tilde{U}_{\mathrm{DD}}^{\alpha} = \frac{1}{2N_\alpha}\sum_{i=1}^{N_\alpha}\sum_{j\neq i}^{N_\alpha} u_{\mathrm{DD}}(ij)$$
$$= \frac{1}{2N_\alpha}\sum_{i=1}^{N_\alpha}\sum_{j\neq i}^{N_\alpha}[(\boldsymbol{\mu}_i\cdot\boldsymbol{\mu}_j)B(r_{ij},\tilde{\alpha}) - (\boldsymbol{\mu}_i\cdot\mathbf{r}_{ij})$$
$$\times(\boldsymbol{\mu}_j\cdot\mathbf{r}_{ij})C(r_{ij},\tilde{\alpha})] + \frac{1}{2N_\alpha V_c}\sum_{\mathbf{k}\neq 0}\frac{4\pi}{k^2}\exp\left(-\frac{k^2}{4\tilde{\alpha}}\right)$$
$$\times\tilde{M}_\alpha(\mathbf{k})\tilde{M}_\alpha^*(\mathbf{k}) + \frac{2\pi}{N_\alpha V_c}\sum_{i=1}^{N_\alpha}\sum_{j=1}^{N_\alpha}\mu_{i,z}\mu_{j,z} - \frac{2\tilde{\alpha}}{3\sqrt{\pi}}\mu^2. \tag{A1}$$

In Eq. (A1), V_c is the volume of the total Ewald cell including the vacuum contribution [25] used in the simulations, that is, $V_c = V + V_{\mathrm{vacuum}}$. Also, $\tilde{\alpha}$ is the convergence parameter, and the functions B and C appearing in the first term on the right-hand side are defined elsewhere (see, e.g., [20]). Furthermore,

$$\tilde{M}_\alpha(\mathbf{k}) = \sum_{i=1}^{N_\alpha}\boldsymbol{\mu}_i\cdot\mathbf{k}\exp(i\mathbf{k}\cdot\mathbf{r}_i). \tag{A2}$$

On the other hand, the (normalized) interaction energy between two different layers α and $\beta\neq\alpha$ is given by

$$\tilde{U}_{\mathrm{DD}}^{\alpha\beta} = \frac{1}{N}\sum_{i=1}^{N_\alpha}\sum_{j=1}^{N_\beta} u_{\mathrm{DD}}(ij)$$
$$= \frac{1}{N}\sum_{i=1}^{N_\alpha}\sum_{j=1}^{N_\beta}[(\boldsymbol{\mu}_i\cdot\boldsymbol{\mu}_j)B(r_{ij},\tilde{\alpha}) - (\boldsymbol{\mu}_i\cdot\mathbf{r}_{ij})(\boldsymbol{\mu}_j\cdot\mathbf{r}_{ij})C(r_{ij},\tilde{\alpha})]$$
$$+ \frac{1}{NV_c}\sum_{\mathbf{k}\neq 0}\frac{4\pi}{k^2}\exp\left(-\frac{k^2}{4\tilde{\alpha}}\right)\frac{1}{2}[\tilde{M}_\alpha(\mathbf{k})\tilde{M}_\beta^*(\mathbf{k})$$
$$+ \tilde{M}_\beta(\mathbf{k})\tilde{M}_\alpha^*(\mathbf{k})] + \frac{4\pi}{NV_c}\sum_{i=1}^{N_\alpha}\sum_{j=1}^{N_\beta}\mu_{i,z}\mu_{j,z}. \tag{A3}$$

[1] M. Klokkenburg, R. P. A. Dullens, W. K. Kegel, B. H. Erne, and A. P. Philipse, Phys. Rev. Lett. **96**, 037203 (2006).
[2] M. Klokkenburg, B. H. Erne, J. D. Meeldijk, A. Wiedenmann, A. V. Petukhov, R. P. A. Dullens, and A. P. Philipse, Phys. Rev. Lett. **97**, 185702 (2006).
[3] J. Richardi, D. Ingert, and M. P. Pileni, Phys. Rev. E **66**, 046306 (2002).
[4] Y. Lalatonne, J. Richardi, and M. P. Pileni, Nature Mater. **3**, 121 (2004).
[5] K. De'Bell, A. B. MacIsaac, and J. P. Whitehead, Rev. Mod. Phys. **72**, 225 (2000).
[6] K. Zahn, R. Lenke, and G. Maret, Phys. Rev. Lett. **82**, 2721 (1999).
[7] O. D. Velev and K. H. Bhatt, Soft Matter **2**, 738 (2006).
[8] N. Osterman, D. Babic, I. Poberaj, J. Dobnikar, and P. Ziherl, Phys. Rev. Lett. **99**, 248301 (2007).
[9] V. Germain, J. Richardi, D. Ingert, and M. P. Pileni, J. Phys. Chem. B **109**, 5541 (2004).
[10] W. Wen, L. Zhang, and P. Sheng, Phys. Rev. Lett. **85**, 5464 (2000).
[11] P. D. Duncan and P. J. Camp, J. Chem. Phys. **121**, 11322 (2004).
[12] J.-J. Weis, Mol. Phys. **103**, 7 (2005).
[13] V. A. Froltsov and S. H. L. Klapp, J. Chem. Phys. **124**, 134701 (2006).
[14] C. Alvarez, M. Mazars, and J. J. Weis, Phys. Rev. E **77**, 051501 (2008).
[15] R. A. Trasca and S. H. L. Klapp, J. Chem. Phys. **129**, 084702 (2008).
[16] J. Richardi, M. P. Pileni, and J.-J. Weis, Phys. Rev. E **77**, 061510 (2008).
[17] B. Reimann, R. Richter, and I. Rehberg, Phys. Rev. E **65**, 031504 (2002).
[18] A. Vorobiev, J. Major, H. Dosch, G. Gordeev, and D. Orlova, Phys. Rev. Lett. **93**, 267203 (2004).
[19] J. Jordanovic and S. H. L. Klapp, Phys. Rev. Lett. **101**, 038302 (2008).
[20] M. P. Allen and D. J. Tildesley, *Computer Simulation of Liquids* (Academic, London, 1987).
[21] M. E. van Leeuwen and B. Smit, Phys. Rev. Lett. **71**, 3991 (1993).
[22] J. Bartke and R. Hentschke, Phys. Rev. E **75**, 061503 (2007).
[23] M. Schoen and S. H. L. Klapp, in *Reviews in Computational Chemistry*, edited by K. B. Lipkowitz and T. Cundari (Wiley-VCH, New Jersey, 2007), Vol. 24.
[24] I.-C. Yeh and M. L. Berkowitz, J. Chem. Phys. **111**, 3155 (1999).
[25] S. H. L. Klapp and M. Schoen, J. Chem. Phys. **117**, 8050 (2002).
[26] S. H. L. Klapp, Mol. Simul. **32**, 609 (2006).
[27] A. F. Pshenichnikov and V. V. Mekhonoshin, Phys. Solid State **40**, 970 (1998).
[28] R. A. Trasca and S. H. L. Klapp, J. Chem. Phys. **129**, 084702 (2008).
[29] M. E. Van Leeuwen, B. Smit, and E. M. Hendriks, Mol. Phys. **78**, 271 (1993).
[30] V. A. Froltsov and S. H. L. Klapp, J. Chem. Phys. **126**, 114703 (2007).
[31] R. Tao and J. M. Sun, Phys. Rev. A **44**, R6181 (1991): Phys. Rev. Lett. **67**, 398 (1991).
[32] D. Wei and G. N. Patey, Phys. Rev. Lett. **68**, 2043 (1992).
[33] P. J. Camp, Phys. Rev. E **68**, 061506 (2003).